© creative

Scientific paper

# Synthesis, DFT, and Molecular Docking Studies of Anti-cancer Imidazolidine-2,4-dione and Thiazolidine-2,4-dione Derivatives

#### Osama Alharbi

 $^1$  Department of Chemistry, College of Science, Taibah University, Al-Madinah Al-Munawwarah, 30002, Saudi Arabia

\* Corresponding author: E-mail: oamharbi@taibahu.edu.sa

Received: 05-14-2025

#### Abstract

Novel families of thiazolidine-2,4-dione and imidazolidine-2,4-dione derivatives were synthesized. Thiazolidine-2,4-dione 3 was prepared using chloroacetic acid and thiourea, followed by condensation with terephthalaldehyde to form 4-((2,4-dioxothiazolidine-5-ylidene)methyl)benzaldehyde 4. This compound reacted with 2-aryloxyacetohydrazides 8a-b to yield Schiff bases 9a-b. Imidazolidine-2,4-diones 13a-c were synthesized via cyclizing of anilines 10a-c, urea 11, and chloroacetic acid 12. The compounds 9a-b and 13a-c were evaluated for antitumor activity against the Caco-2 cell line, compounds 13b and 13c exhibiting the highest potency ( $IC_{50}$  values of 41.30  $\pm$  0.07  $\mu$ M and 109.2  $\pm$  0.027  $\mu$ M, respectively). DFT calculations, including HOMO-LUMO analysis, energy gap estimation, and molecular docking, were conducted to evaluate and optimize the molecular properties of the target compounds.

Keywords: Imidazolidine-2,4-dione; thiazolidine-2,4-dione; molecular docking; DFT; anti-cancer.

#### 1. Introduction

Tumors are a category of intricate disorders described by the rapid, unregulated, and serious cell proliferation, which disrupts the process of normal cell division.<sup>1</sup> It is considered one of the gravest diseases threatening human health. Improved recognition of the complicated nature of cancer biology has been critical in the advancement of cancer therapies. Recent research has focused on developing novel cancer therapies using non-toxic therapeutic approaches.<sup>2</sup> Chemotherapy, a widely used cancer treatment, works by interfering with the mechanisms regulating cell division. Its goal is to prevent metastasis and invasion by inhibiting tumor growth. However, chemotherapy can cause adverse side effects due to its impact on healthy cells. Key challenges in cancer treatment include drug resistance and adverse off-target effects, driving the development of new anti-cancer agents with minimal toxicity and high efficacy.3 Heterocyclic scaffolds are valued in medicinal and synthetic organic chemistry for their diverse biological activities and chemical versatility.<sup>4,5</sup> These compounds, derived from natural sources or synthetic methods, have significant potential in overcoming drug resistance and improving treatment efficacy. Notably, thiazolidine-2,4-diones, commonly known as glitazones, are

a class of heterocyclic compounds exemplified by the archetypal medication ciglitazone. These compounds are used in the management of type 2 diabetes mellitus, introduced in the late 1990s.6 In addition to their antidiabetic efficacy, thiazolidine-2,4-diones inhibit the proliferation of various cancer cell lines, including colon, breast, and prostate, both in vivo and in vitro. 7,8 Thiazolidine-2,4-dione is a highly selective oral agonist of peroxisome proliferator-activated receptor gamma (PPARy), which shown potential in stabilizing disease progression in patients with metastatic colorectal cancer (mCRC), along with demonstrating favourable safety and pharmacokinetic stability.9 Imidazolidine-2,4-dione and thiazolidine-2,4-dione are significant five-membered heterocycles characterized by two carbonyl groups. These groups impart unique electronic and steric properties, making them valuable synthetic intermediates and pharmacophores in medicinal chemistry. The incorporation of nitrogen and sulfur in these frameworks significantly affects their nucleophilic, electrophilic, and tautomeric properties, thus regulating their reactivity and applications. The imidazolidine-2,4-dione ring is a key pharmacophore with diverse biological properties. 10 Its derivatives are well-known for anticonvulsant, antiarrhythmic, antibacterial, skeletal muscle relaxant, and non-steroidal antiandrogen properties. Imidazolidine-2,4-dione and its analogues are found in some naturally occurring compounds, such as certain alkaloids. Numerous alkaloids containing an imidazolidine-2,4-dione ring, such as the aplysinopsins, have been isolated from sponges or corals and demonstrate potent biological activity, including antimicrobial and cytotoxic effects. <sup>10</sup> Building on the diverse therapeutic potential of imidazolidine-2,4-dione and thiazolidine-2,4-dione derivatives, this study investigates novel approaches to enhance cancer treatment by synthesizing and evaluating new derivatives for their anti-cancer activity. <sup>11</sup>

#### 2. Experimental

#### 2. 1. Materials and Methods

All chemical reagents were of analytical grade and purchased from Accela ChemBio Co., Ltd. (Shanghai, China). Melting points have been determined using an XT-4 melting point instrument (Beijing Tech Instrument Co., China).  $^{1}$ H and  $^{13}$ C NMR were recorded on an AVANCE III HD 400 MHz NMR spectrometer (Bruker Corporation, Switzerland.) or JEOL ECX 500 MHz NMR spectrometer (JEOL Ltd., Japan) operating at room temperature, using DMSO- $d_6$  or CDCl $_3$  as solvents. Reaction progress was monitored by thin-layer chromatography (TLC). FT-IR spectra were recorded on a Nicolet iS5 FTIR spectrophotometer (Thermo Fisher Scientific, USA) using KBr pellets.

#### 2. 2. Synthesis of Thiazolidin-2,4-dione (3)<sup>12</sup>

The established procedure was followed to synthesize compound 3. Chloroacetic acid (9.45 g, 0.1 mol) and thiourea (7.61 g, 0.1 mol) were dissolved in 10 mL of  $\rm H_2O$  and stirred for 15 minutes until a white precipitate formed. The mixture was cooled, and 10 mL of concentrated HCl was slowly added. The flask was then attached to a reflux condenser, and the mixture was refluxed with stirring at 100–110 °C for 8–10 hours. The product was cooled, filtered, washed, dried at room temperature, and recrystallized from water to yield a white solid. Melting point: 115 °C; yield: 11.11 g (95%).

# 2. 3. Synthesis of 4-((2,4-dioxothiazolidine-5-ylidene)methyl)benzaldehyde (4)<sup>13</sup>

A mixture containing compound 1 (0.03 mol), terephthalaldehyde (0.03 mol), and 45 mL of ethanol was prepared. Piperidine (3 mL, 0.0188 mol) was added, and the solution was stirred and refluxed for 12 hours. The reaction mixture was then poured onto ice and acidified using glacial acetic acid. This process yielded a yellow substance identified as compound 4, which was subsequently filtered, dried, and purified through recrystallization using ethanol.

# 2. 4. Synthesis of Ethyl 2-substituted-oxyacetate 7a-b<sup>13,14</sup>

In 65 mL of anhydrous acetone, hydroxy aromatic compounds (5a–b, 0.034 mol), anhydrous  $K_2CO_3$  (4.72 g, 0.034 mol), and chloroethyl acetate (2, 4.2 g, 0.034 mol) were refluxed for 8–10 h. After completion, the solvent was removed under reduced pressure, and the residue was dissolved in dichloromethane (DCM, 20 mL) and washed with water. The organic layer was evaporated to yield compounds 7a and 7b as solids, with yields of 84% (7a) and 92% (7b), respectively.

## 2. 5. Synthesis of 2-(substituted-2-yloxy) acetohydrazide 8a-b<sup>13-15</sup>

The hydrazine hydrate (0.75 g; 0.015 mol) was added dropwise to solution of **7a** or **7b** (0.015 mol) in ethanol (25 mL). The resulting mixture was subjected to ultrasonic irradiation at ambient temperature for 0.5 h. The solid was filtered and dried to produce compounds **8a**, Yield: 45%; m.p. 220–222 °C; **8b**, Yield: 60%; m.p. 242–243 °C.

#### 2. 6. Synthesis of Compounds (9a-b)

Using a catalytic quantity of glacial acetic acid, substituted hydrazides **8a** or **8b** (0.01 mol) were added to a solution of compound **4** (0.01 mol) in methanol (50 mL), and the obtained mixture was refluxed for 4–18 h. The final compounds (**9a-b**) were obtained by recrystallizing the reaction mixture from methanol after it had cooled.

# Synthesis of 2-((3,6-dioxocyclohexa-1,4-dien-1-yl)ox-y)-N'-(4-(-(2,4-dioxothiazolidin-5-ylidene)methyl)ben-zylidene)acetohydrazide (9a)

Brown solid; Yield: 45%; m.p. 220–224 °C.; FT-IR  $v_{\text{max}}$  (KBr)/cm<sup>-1</sup> 3367, 3186 (NH), 1774, 1716, 1678 (C=O); <sup>1</sup>H NMR (DMSO- $d_6$ ):  $\delta$  4.57 (s, 2H, CH<sub>2</sub>), 7.27–8.02 (m, 9H, CH=C, H-Ar), 11.71, 11.76 (s, 2H, NH). <sup>13</sup>C NMR (DMSO- $d_6$ ):  $\delta$  52.10, 116.22, 129.68,131.50, 143.82, 146.87, 162.91, 163.51, 165.14, 165.43; Anal. Calcd. for C<sub>19</sub>H<sub>13</sub>N<sub>3</sub>O<sub>6</sub>S (411.05): C, 55.47; H, 3.19; N, 10.21; Found: C, 55.52; H, 3.09; N, 10.29%.

# Synthesis of $N^2$ -(4-(-(2,4-dioxothiazolidin-5-ylidene) methyl)benzylidene)-2-(naphthalen-1-yloxy)acetohydrazide (9b).

Pale brown solid; Yield: 60%; m.p. 243 °C; FT-IR  $v_{\rm max}$  (KBr)/cm<sup>-1</sup> 3323–3257(N-H), 3098–3021 (C-HAr), 2967–2911 (C-HAliph), 1709–1619 (C=O), 1651–1624 (C=N) 1645–1625 (C=C); <sup>1</sup>H NMR (DMSO- $d_6$ ): δ 4.98 (s, 1H, NH), 5.30 (s, 2H, CH<sub>2</sub>), 6.40–7.95 (m, 13H, C=CH, H-Ar), 11.73 (s, 1H, NH). <sup>13</sup>C NMR (DMSO- $d_6$ ): δ 62.54, 105.99, 121.21, 125.76, 125.95, 126.46, 126.55, 127.89, 127.94, 134.56, 154.11, 162.86, 172.54; Anal. Calcd. for C<sub>23</sub>H<sub>17</sub>N<sub>3</sub>O<sub>4</sub>S (431.09): C, 64.03; H, 3.90; N, 9.74; Found: C, 64.13; H, 3.99; N, 9.94%.

# 2. 7. Synthesis of 3-phenyl-2-(phenylimino) imidazolidin-4-one derivatives (13a-c)

A mixture of phenylamine (0.01 mol, 0.94 g), urea (0.01 mol, 0.69 g), and chloroacetic acid (0.01 mmol, 0.95 g was stirred for 30 minutes. The resulting mixture underwent trituration with hot, diluted methanol solution in distilled water. After cooling, the precipitated solid was separated through filtration, subjected to drying, and subsequently recrystallized using ethanol as solvent, producing buff-coloured crystalline material identified as compound 13a-c.

#### Synthesis of 2-((4-chlorophenyl)imino)-3-phenylimidazolidin-4-one (13a)

Pale brown solid; Yield: 53%; m.p. 277–280 °C; FT-IR  $v_{\rm max}({\rm KBr})/{\rm cm}^{-1}$  3310–3277 (N-H), 3100–3001 (C-H, Ar), 2997–2941 (C-H, Aliph), 1733–1649 (C=O), 1649–1627 (C=N), 1635–1619 (C=C); <sup>1</sup>H NMR (DMSO- $d_6$ ): δ 3.90 (s, 2H, CH<sub>2</sub>), 6.17–7.62 (m, 9H, H-Ar). <sup>13</sup>C NMR (DMSO- $d_6$ ): δ 52.09, 114.00, 115.70, 120.13, 120.20, 121.32, 129.01, 138.17, 147.50, 172.04; Anal. Calcd. for C<sub>15</sub>H<sub>12</sub>ClN<sub>3</sub>O (285.07): C, 63.05; H, 4.23; N, 14.71; Found: C, 63.12; H, 4.16; N, 14.63%.

### Synthesis of 2-((4-bromophenyl)imino)-3-phenylimidazolidin-4-one (13b)

Pale brown solid; Yield: 66%; m.p 281–285°C; FT-IR  $v_{\rm max}({\rm KBr})/{\rm cm}^{-1}$  3301–3282 (N-H), 3099–3001(C-H, Ar), 2997–2941(C-H, Aliph), 1731–1656 (C=O), 1649–1627 (C=N), 1625–1619 (C=C);  $^1{\rm H}$  NMR (DMSO- $d_6$ ):  $\delta$  3.90 (s, 2H, CH<sub>2</sub>), 6.20–7.57 (m, 9H, H-Ar) .  $^{13}{\rm C}$  NMR (DMSO- $d_6$ ):  $\delta$  52.10, 107.50, 114.58, 114.60, 114.41, 114.74, 116.27, 121.70, 131.78, 131.83, 132.01, 132.67, 138.59, 147.87, 172.00; Anal. Calcd. for  $C_{15}{\rm H}_{12}{\rm BrN}_3{\rm O}$  (329.02): C, 54.56; H, 3.66, N, 12.73; Found: C, 54.66; H, 3.78, N, 12.85%.

#### Synthesis of 2-((4-acetylphenyl)imino)-3-phenylimidazolidin-4-one (13c)

Pale brown solid; Yield: 43%; m.p. 279–284 °C; FT-IR  $v_{\rm max}$ (KBr)/cm<sup>-1</sup>; 3313–3267 (N-H), 3108–3021(C-H, Ar), 2977–2921 (C-H, Aliph), 1713–1619 (C=O), 1654–1619 (C=N) 1645–1625 (C=C; <sup>1</sup>H NMR (DMSO- $d_6$ ): δ 1.65 (s, 3H, CH<sub>3</sub>), 4.40 (s, 2H, CH<sub>2</sub>), 7.47–8.21 (m, 9H, C=CH, H-Ar), 11.71(s, 1H, NH). <sup>13</sup>C NMR (DMSO- $d_6$ ): δ 22.49, 50.85, 128.54, 129.04, 129.38, 133.34, 133.37, 134.50, 134.86, 143.00, 146.43, 169.34, 171.25; Anal. Calcd. for C<sub>17</sub>H<sub>15</sub>N<sub>3</sub>O<sub>2</sub> (293.12): C, 69.61; H, 5.15; N, 14.33; Found: C,-70.11; H, 5.45; N, 14.67%.

#### 2.8. Biological Evaluation

#### 2. 8. 1. Cell Culture

Human splenic fibroblast (HSF) and human colonic epithelial (Caco-2) cell lines, obtained from the National Cancer Institute in Egypt, were cultivated in RPMI 1640 or

DMEM media (Gibco, USA) with a 10% fetal bovine serum added (Hyclone, USA). At 70–80% confluence, cells were harvested using a 0.25% trypsin/EDTA cocktail and planted into a fresh culture flask containing DMEM-LG with 10% FBS and 0.1 mg/mL primocin. Flask were then incubated at 37 °C with 5% CO<sub>2</sub>. Cells were passaged every 5–6 days, and the media was replaced every 48 hours. <sup>13,15</sup>

#### 2. 8. 2. MTT Assay

Using the MTT assay, recently synthesized compounds (9a-b, 13a-c) were evaluated for cytotoxicity against normal human skin fibroblasts (HSF) and malignant Caco-2 cell lines, the latter derived from human colorectal adenocarcinoma and serving as a standard *in vitro* model for colorectal cancer. These compounds had not previously been tested against Caco-2 in this context, making this study novel in assessing their anticancer activity in a colorectal cancer model. The results, particularly for 13b and 13c, demonstrated significant cytotoxicity and selectivity, supporting their potential as anticancer agents.

The MTT assay was used to assess the cytotoxicity of compounds **9a-b** and **13a-c** by measuring cell viability via mitochondrial reduction of yellow tetrazolium salt to purple formazan crystals. Cells were plated at a density of 1  $\times$  10<sup>4</sup> cells/well in 96-well plates and incubated at 37 °C with 5% CO<sub>2</sub>. They were then exposed to test compounds at concentrations of 0–500  $\mu M$  for 48 hours. After incubation with 10  $\mu L$  of MTT solution for 4 hours, 100  $\mu L$  of solubilization solution (e.g., DMSO) was added to dissolve the formazan, and absorbance was measured at 490 nm. Experiments were conducted in biological triplicate, with untreated control cells set as 100% viability. IC50 values were analyzed using GraphPad Prism 5.0.

#### 2. 9. Docking Simulation

AutoDockTools-1.5.6rc3 (ADT4),16 was adopted for in silico molecular docking toward calculate the compelling modes of potent 13b through selected proteins. ADT4 has been widely reported as one of the best docking tools for structure-based drug design and virtual screening of drug-like molecules through the prediction of how the ligands can interact with protein targets to obtain the possible effective interactions between them. 17-19 In the current docking, we have used Bcl-2 protein (PDBID: 4IEH) which is recognized as a target for anti-cancer compounds, especially with colorectal cancer. 19-21 The 3D structure data of Bcl-2 protein target proteins were obtained in pdb, format from RCSB- PDB internet site (http://www.rcsb. org/pdb/). Besides, the compound 13b was built and refined in 3D-Chem Draw Ultra 12.0 and minimized energetically by MM2 force field before saving in pdb. file. Prior of the docking, the target protein has been prepared by deleting all water, co-crystal ligand and co-factors. As well, ADT4 was utilized to set polar hydrogens, charge deactivations and rotatable bonds. The computer simulation of ligand-protein was achieved under Lamarckian Genetic Algorithm (LGA) technique. The docking grid box [110  $\times$  110  $\times$  110 Å<sup>3</sup>] was run at the active site pocket of the Bcl-2 protein. The prediction analysis of docking results was carefully done under strict settings with RMSD  $\leq$  2.0Å. This effects for modern docking exposed possible H-bonds as well as binding energy interactions of our compound with the Bcl-2 protein. The parameters of five orientations are recorded in **Table 2**. Along with ADT4, both PyMOL and BIOVIA software were also used for the analysis and visualization of the results.  $^{22-24}$ 

#### 2. 10. Density Functional Theory (DFT)

The computational function within the current test was done through using DFT-B3LYP efficient under 6-311++G(d,p) bases organized which is considered as one of the best computational quantum models used with organic compounds.<sup>25,26</sup> DFT-B3LYP/6-311++G(d,p) combination has proven high degree of accuracy in the geometric optimization, energies, electronic structure and correlated molecular characteristics.<sup>26–28</sup> Owing to the relation between the reactivity features and biological behaviours of the compound, DFT-B3LYP/6-311++G(d,p) was employed to calculate the verves of lowest- unoccupied/highest employed molecular orbitals (LUMO-HO-MO) which are recognized as (FMOs = frontier molecular orbitals). Based on the FMOs, we have also computed the energy gap ( $\Delta E_{gap}$ ) and other parameters of chemical reactivities like; international electrophilicity index  $\psi$ , global hardness  $\eta$ , electronegativity  $\chi$ , electronic chemical potential  $\mu$  and global softness  $\zeta$ . Moreover, the molecular electrostatic potential (MEP) of the computed compound was also explored under the same computational combination. All the DFT studies, in the present work, were executed in

Gaussian 09 program.<sup>29</sup> While the construction of structure input file and figure visualizations have been done using GaussView5 program.<sup>13,30</sup>

#### 3. Results and Discussion

#### 3. 1. Rationale of the Study

This study builds on the well-documented pharmacological potential of thiazolidine-2,4-dione and imidazolidine-2,4-dione scaffolds, both recognized for their broad spectrum of biological activities, particularly in cancer therapy (Figure 1). Previous research by El-Adl et al. described the development of thiazolidine-2,4-dione-based compound A, which demonstrated superior anticancer efficacy compared to a reference drug against HepG2, HCT-116, and MCF-7 cell lines.<sup>30</sup> Similarly, Mahmoud et al. reported the synthesis of novel imidazolidine-2,4-dione derivatives, derivative B, which exhibited significant cytotoxicity against MCF-7 and A549 cell lines, surpassing the activity of the standard treatment. Inspired by the robust anticancer profiles of these scaffolds, the present study introduced strategic modifications to enhance their therapeutic performance. This approach successfully yielded compounds 13b and 13c, both showing notable inhibitory activity in vitro.

#### 3. 2. Chemistry

In this study, we synthesized novel imidazolidine-2,4-dione as well as thiazolidine-2,4-dione derivatives via synthetic pathway shown in Schemes 1. The production of thiazolidine-2,4-dione 3 has been accomplished by an established literature procedure using chloro-acetic acid and thiourea in the presence of HCl as catalyst.<sup>31</sup> Consequently, Knoevenagel condensation of thiazoli-

Figure 1. Examples of the well-documented pharmacological potential of thiazolidine-2,4-dione and imidazolidine-2,4-dione scaffolds.

din-2,4-dione **3** with equivalent amount of terephthalaldehyde was performed resulting in the formation of 4-((2,4-dioxothiazolidine-5-ylidene)-methyl)-benzaldehyde **4** in the presence of piperidine.<sup>31</sup>

In this study, the key intermediate compounds, substituted ethyl 2-aryloxyacetates (7a-b), were synthesized efficiently with good yields by reacting ethyl 2-chloroacetate (6) with substituted hydroxy compounds (5a-b, as detailed in Scheme 1) using anhydrous potassium carbonate in dry acetone. These intermediates were then reacted with hydrazine hydrate in ethanol to yield substituted 2-aryloxyacetohydrazides (8a-b) with yields of 84 and 92%. 32,33 In the final step, 4-((2,4-dioxothiazolidin-5-ylidene)methyl)benzaldehyde (4) was refluxed with 2-aryloxyacetohydrazides (8a-b) in absolute ethanol with a catalytic amount of acetic acid for 4–5 hours, forming Schiff bases (9a-b), as illustrated in Scheme 1.

In Scheme 2, the target molecules **13a-c** were synthesized by one-pot condensation reaction of aniline deriva-

tives **10a-c**, urea **11**, and chloro-acetic acid **12** which undergo cyclization without solvent to produce *N*-phenylimidazole, followed by condensation with another molecule of aniline to furnish 3-phenyl-2-(phenylimino)imidazolidin-4-one **13a-c**.

All the target compounds were structurally confirmed through IR, <sup>1</sup>H and <sup>13</sup>C NMR spectroscopy. The formation of Schiff base compound **9a** was confirmed by IR spectroscopy, which revealed a C=N stretching band at 1649 cm<sup>-1</sup> and two carbonyl stretching bands at 1626 and 1635 cm<sup>-1</sup>, consistent with conjugated carbonyl groups. The <sup>1</sup>H NMR spectrum showed signals at 11.71 and 11.76 ppm, assigned to two NH proton Additionally, new signals were observed in the range of 7.27–8.02 ppm, attributed to C=CH and aromatic protons. The IR spectrum of compound **13a** revealed bands at 3282 and 3292 cm<sup>-1</sup> assigned to NH stretching and a band at 1639 cm<sup>-1</sup> assigned to C=N stretching. The <sup>1</sup>H NMR spectrum displayed a signal at 3.90 ppm attributed to the CH<sub>2</sub> group and signals in the

$$X$$

NH<sub>2</sub>

NH<sub>2</sub>

NH<sub>2</sub>

NH<sub>2</sub>

NNH

NH

NNH

NH

NAH

10a-c

11

12

Scheme 2. Synthesis of compounds 13a-c

X= CI, Br, - COCH<sub>3</sub>

range of 6.20–7.57 ppm corresponding to aromatic protons, consistent with the proposed structure.<sup>32,33</sup>

#### 3. 3. Biological Assays

#### 3. 3. 1. Cytotoxicity Assay

This study investigated the in vitro cytotoxic activity of all selected compounds (9a-b and 13a-c) against normal (HSF) and cancer (Caco-2) cell lines. All tested compounds exhibited cytotoxicity against Caco-2 cells, with  $IC_{50}$  values ranging from  $40.67 \pm 0.09$  to  $109.2 \pm 0.027 \,\mu\text{M}$ (Table 1). Compounds 13b and 13c showed higher cytotoxicity, with IC<sub>50</sub> values of 41.30  $\pm$  0.07  $\mu$ M and 109.2  $\pm$ 0.027 µM, respectively. Compounds 13a and 9a displayed moderate cytotoxicity, with IC<sub>50</sub> values of  $40.67 \pm 0.09 \,\mu\text{M}$ and  $66.68 \pm 0.068 \mu M$ , respectively, while compound 9b exhibited less potent cytotoxicity, with an IC<sub>50</sub> value of  $73.91 \pm 0.03 \,\mu\text{M}$ . To address IC<sub>50</sub> values exceeding 500  $\mu\text{M}$ , particularly for HSF cells, compounds 9a-b and 13a-c were tested using a two-fold serial dilution from 15.625 to 1000 μM. Compounds with low cytotoxicity against HSF cells (e.g., 13b, 13c) were evaluated at higher concentrations, despite initial screening up to 500 µM. IC<sub>50</sub> values were calculated using GraphPad Prism 5.0 based on full dose-response curves, with data points up to 1000 µM ensuring accurate determination for compounds like 13c, which showed low inhibition below 500 µM. All compounds were soluble in culture medium with ≤0.5% DM-SO, showing no precipitation or turbidity, ensuring no vehicle-related cytotoxicity. Caco-2 and HSF cell lines were treated under identical conditions (seeding density, incubation time, medium composition, assay procedures) to ensure data consistency and comparability, validating the reported IC<sub>50</sub> and selectivity index values.

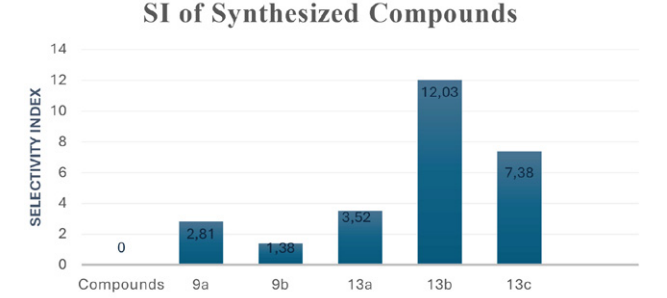
**Table 1.** In vitro cytotoxicity (IC $_{50}$ ) of compounds **9a-b** and **13a-c** against HSF and Caco-2 cell lines using the MTS assay.

| Compound | $IC_{50} \pm SI$ | D* (μM)     | SI for Caco-2 |
|----------|------------------|-------------|---------------|
|          | HSF              | Caco-2      |               |
| 9a       | 187.3±0.014      | 66.68±0.068 | 2.81          |
| 9b       | 102.1±0.11       | 73.91±0.036 | 1.38          |
| 13a      | 143.4±0.022      | 40.67±0.09  | 3.52          |
| 13b      | 496.8±0.041      | 41.30±0.07  | 12.03         |
| 13c      | 805.9±0.05       | 109.2±0.027 | 7.38          |

 $^*IC_{50}$ : Concentration of the compound resulting in 50% suppression of cell growth  $\pm$  standard deviation.

The selectivity index (SI), defined as the ratio of  $IC_{50}$  values for normal (HSF) to cancer (Caco-2) cell lines, was calculated and presented in Figure 2 and Table 1. SI values greater than 2.0 indicate higher selectivity for cancer cells.<sup>34</sup> According to the results, compound **9b** with SI of 1.38 suggests that it has comparable effects on malignant

and healthy cells, which limits its usefulness as a selective anticancer agent. Because cancer cells do not exhibit a markedly increased cytotoxicity, the use of this compound in therapy may result in significant toxicity to normal cells, raising the possibility of adverse effects. On the other hand, compound 9a demonstrates moderate selectivity (SI = 2.81), indicating that although the chemical is more harmful to cancerous cells than cells that are normal, the difference is not very large. This indicates that the possibility of cytotoxic effects on healthy cells remains at therapeutic dosages. Compound 13a, with an SI of 3.52, demonstrated moderate selectivity for Caco-2 cells over HSF cells, making it a promising candidate for further preclinical anticancer studies. According to this, the compound is substantially more cytotoxic to cancer cells than healthy cells, which makes it an attractive option for more preclinical study in anticancer investigations. Compounds 13b and 13c exhibited SI values of 12.02 and 7.38, respectively, for Caco-2 cells relative to HSF cells, indicating higher selectivity with significantly greater cytotoxicity toward cancer cells than normal cells (Figure 2). These results position both compounds as promising candidates for further anticancer drug development.35



SI of synthesized compounds

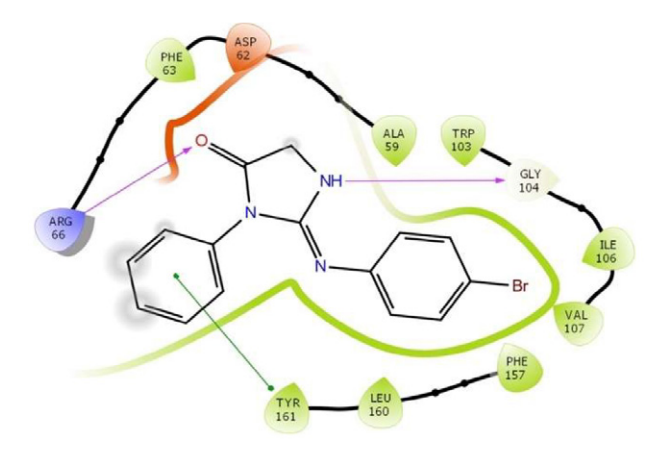
SYNTHESIZED COMPOUNDS

Figure 2. SI of synthesized compounds.

#### 3. 3. 2. Docking Simulation

The molecular docking study was aimed to check the possible effective interactions of potent molecule compound 13b with the Bcl-2 protein receptors. Based on the co-crystal ligand, the typical modes for inhibition binding positions were identified within the Bcl-2 active site, which comprise the interaction of cocrystal ligand (1E9) with ARG66 and GLY104 residues.<sup>20</sup> The outcomes of recent docking exposed rational H-bond connections with our ligand with the effective amino acids of Bcl-2 as listed in Table 2. The greatest binding energy reached (-7.77 kcal/mol) through three H-bond interaction formed as single bond of GLY104 with N14 atom at distance 1.78 Å, as well as double H-bonds linked over-coordinated O29 atom of our ligand with two N atoms of ARG66 residue at distances of 1.78, 1.82 and 2.14 Å forming R<sup>2</sup><sub>1</sub> ring motif which

strengthens the interaction and bond stabilization of protein-ligand. Additionally, this conformation exhibited pipi stacking between HIS432 and the phenyl ring of compound 13b, as shown in Figures 3 and 4. Other conformations (2 and 3) showed hydrogen bonds with ARG66 and PHE63 via the O29 atom (2.17 Å and 2.28 Å, binding energies of -7.71 and -7.69 kcal/mol, respectively). Moreover, the conformations 2 and 3 showed H-bond



**Figure 3.** 2-D interaction plot of the potent molecule compound **13b** docked with 4IEH showing hydrogen bond and pi interactions.

interactions of AGR66 and PHE63 a with the O29 atom at distances 2.17 and 2.28 Å and B.E of -7.71 and -7.69 kcal/ mol. Likewise, TYR161 and GLY104 residues in conformations 4 and 5 shaped H-bonds with N14 atom at distances of 2.15, and 1.97 Å (see Figure **S1** in Supplementary Material). Thus, the bond interactions in our current docking are observed to be parallel to that of co-crystal ligand and reported literature which reflects the perfect settlement of our potent molecule in Bcl-2 active site pocket.<sup>20,21,36</sup> Figure 3 depicts 2D plot of ligand-Bcl2 interactions, while Figure 4 illustrates the enfoldment of ligand inside Bcl-2 active site cleft with zoom view in ribbon and 3D models. Consistently, the computer docking predicted the better B.E values and strong bonding interactions of our potent compound 13b, that might be a favourable candidate for anticancer drugs development.

#### 3. 4. Density Functional Theory (DFT)

#### 3. 4. 1. Geometry Optimization

The structure geometry of compound 13b has been prudently enhanced at stationary point of ground state energy level, which is adopted in all other computations. Furthermore, the stability of optimized geometry has been examined and confirmed by implementing the 'sta-

Table 2. Docking results of the potent molecule 13b compound docked with 4IEH.

| Conf | B.E<br>(kcal/mol) | L.E   | I. C, μM<br>T = 298.15 K | vdW-Hb-<br>des-energy<br>kcal/mol | H-bonds of<br>amino acids<br>with ligand | B.L<br>(Å) | π–Interaction<br>(Å) |
|------|-------------------|-------|--------------------------|-----------------------------------|--|------------|----------------------|
| 1    | -7.77             | -0.39 | 2.03                     | -7.82                             | AGR66NH:                                 | 1.82       | TYR161Cg1            |
|      |                   |       |                          |                                   | O  | 2.14       |                      |
| 2    | -7.71             | -0.39 | 2.23                     | -7.76                             | AGR66NH:O                                | 1.47       |                      |
| 3    | -7.69             | -0.38 | 2.31                     | -7.47                             | PHE63NH:O                                | 2.28       | TYR161 <i>Cg</i> 2   |
| 4    | -7.21             | -0.36 | 5.22                     | -7.55                             | TYR161O:HN                               | 1.45       |                      |
| 5    | -7.07             | -0.35 | 6.56                     | -7.52                             | GLY104O:HN                               | 1.42       | TYR161 <i>Cg</i> 1   |

Conf: Conformation, B.E: Binding Energy, L.E: Ligand Efficiency, I.C: Inhibition Constant, vdW: Vander Walls energy, Hb: Hydrogen bond energy, des: desolv energy, and B.L: Bond length. Cg1 and Cg2 are the centroids of phenyl and bromophenyl rings, respectively.

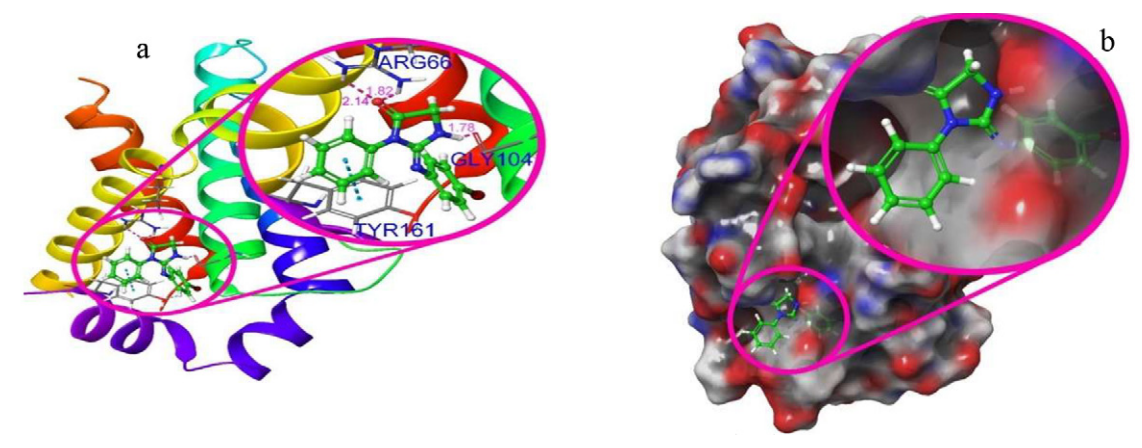


Figure 4. Visualization of whole and close view of the potent molecule compound 13b docked at the active site groove of the protein target a) Ribbon and b) 3D model.

bile" keyword and validated by the nonappearance of negative frequencies, which specified the stationary point computed structure at the ground state. 37,38 The DFT optimized tested form of compound 13b through atoms enumeration is given in Figure 5. The selected computed geometries are recorded in Tables 3-5. Full geometry parameters are given in Tables 3-5 of Supplementary Material. The DFT computed structure of compound 13b exhibited coplanarity conformation between phenyl rings, while the mean plane of imidazole ring is nearly perpendicular to the both phenyl rings as depicted in Figure 5. The torsion angle usually describes the steric connection across the bonds and ring geometries. The imidazole ring is an anti-clinal conformity by point to the phenyl ring, as specified by the rotation angle degree of -125.72° (C28-N13-C17-C18). While the imidazole ring exhibited in +anti-clinal with respect to bromophenyl ring according to the torsion angle of C4-C3-N12-C15 (121.24°). The optimized geometry of compound 13b is in good agreement with the similar reported phenyl-imidazole compounds.<sup>39</sup>

#### 3. 3. 2. Frontier Molecular Orbitals (FMOs)

The reactivity, stability, and electronic transport properties are significantly associated with the values of  $E_H$ ,  $E_L$  and  $\Delta E_{gap}$  which empowers us to explore chemical hardness, softness, and kinetic stability for tested molecules. Typically, the small data for  $\Delta E_{ga}$  reflects the softness which lead toward the easy electronic transportations from HOMO toward LUMO of the molecules, which

**Table 3.** Selected bond lengths( $\hat{a}$ ) of potent compound **13b** computed at dft-b3lyp/6-311++g(d,p)

| Atoms   | Length (Å) | Atoms   | Length (Å) |
|---------|------------|---------|------------|
| C1-C2   | 1.3927     | N14-H16 | 1.008      |
| C1-C6   | 1.3911     | N14-C30 | 1.4511     |
| C3-N12  | 1.4054     | C19-C22 | 1.3925     |
| C4-C5   | 1.3918     | C19-H23 | 1.0822     |
| C4-H9   | 1.0836     | C20-C24 | 1.394      |
| C6-Br11 | 1.9195     | C22-H26 | 1.0839     |
| N12-C15 | 1.2726     | C24-H27 | 1.084      |
| N14-C15 | 1.3792     | C30-H32 | 1.093      |

points to the significant bio-activity of the molecules. Because the biomedical system possess well interaction with soft molecules compared to hard ones. 42 The illustration of LUMO and HOMO populations of 13b are depicted in Figure 6, as (-ve &+ve) stages are introduced in red as well as green, individually. The computed values all reactivity parameters are enumerated in Table 6. The  $E_{H}$  value of HOMO orbital is found to be -3.514 eV with electronic distribution of  $\pi$  character appears over the bromophenyl ring which predictable to involve in pi-pi stacking interaction. In addition, the  $\sigma$  electronic density covered the imidazole ring and bromine moiety, while the other phenyl ring has no electron density. In contrast, the LUMO orbital revealed the main  $\pi$  electronic distribution over the entire molecular system with  $E_L = -1.060$  eV. The DFT values of  $\Delta E_{gap}$  and softness are 2.453 eV and 0.815, respectively. The lower  $\Delta E_{gap}$  value, highest softness degree and main dose of electronic intensity for LUMO compared to LU-MO signifies the easiest of electronic transportation and good reactivity of the molecule in comparison of similar reported compounds.43,44

#### 3. 3. 3. Molecular Electrostatic Potential MEP

The diagram of 3D-MEP illustration at different orientations of our potent molecule is shown in Figure 7. It portrayed in colour system ranging from highest +ve potential (dark blue) to highest –ve potential (deepest red). The highest nucleophilic site (i.e., –ve site) seems round the oxygen atom, so it exists an attractive object for the electrophilic attack to shape acceptor hydrogen bonds. The average –ve sites represented by orange colour and appear over bromine Br11 and nitrogen bridge atom N12 with middling opportunity to construct H-bonds with electrophilic sites. On the other hand, the maximum electrophilic site (i.e., +ve site) appears over the nitrogen atom in imidazole ring N14, so it tends to build donor hydrogen bond during the interaction with nucleophilic substrate-protein interactions, (see docking part).

Besides, the carbon atom in imidazole ring C30 exhibited average +ve site which may also act as hydrogen donor in the interaction with nucleophilic sites. The light green (zero potential) is broadly covering phenyl rings, which tend to shape pi-bonding interactions as demonstrated in docking study.

**Table 4.** Selected bond angles (°) of potent compound **13b** computed at dft-b3lyp/6-311++g(d,p)

| Atoms     | Angle (°) | Atoms       | Angle (°) | Atoms       | Angle (°) | Atoms       | Angle (°) |
|-----------|-----------|-------------|-----------|-------------|-----------|-------------|-----------|
| C2-C1-C6  | 119.46    | C6-C5-H10   | 120.36    | N13-C17-C18 | 120.23    | C24-C22-H26 | 120.22    |
| C2-C1-H7  | 120.16    | C1-C6-C5    | 120.75    | N13-C17-C19 | 119.21    | C20-C24-C22 | 119.81    |
| C2-C3-C4  | 118.34    | C15-N13-C28 | 111.52    | C17-C19-C22 | 119.57    | O29-C28-C30 | 126.58    |
| C2-C3-N12 | 122.24    | C17-N13-C28 | 123.91    | C17-C19-H23 | 119.9     | N14-C30-C28 | 102.71    |
| C3-C4-H9  | 118.9     | H16-N14-C30 | 122.49    | C18-C20-H25 | 119.51    | C28-C30-H31 | 109.08    |
| C4-C5-C6  | 119.43    | N12-C15-N14 | 130.23    | C19-C22-C24 | 120.24    | H31-C30-H32 | 108.59    |

**Table 5.** Selected torsion angles (°) of potent compound **13b** computed at dft-b3lyp/6-311++g(d,p)

| Atoms         | Angle (°) | Atoms            | Angle (°) | Atoms              | Angle (°) |
|---------------|-----------|------------------|-----------|--------------------|-----------|
| C6-C1-C2-C3   | -0.05     | C3-N12-C15-N14   | -3.26     | N13-C17- C19-C22   | -179.01   |
| C2-C1-C6-Br11 | -179.94   | C15-N13-C17-C18  | 55.4      | C17- C18- C20- H25 | 179.59    |
| H7-C1-C6-C5   | -178.99   | C15-N13-C17-C19  | -125.58   | H21-C18-C20-C24    | -179.59   |
| H7-C1-C6-Br11 | 0.5       | C28- N13-C17-C18 | -125.72   | H21-C18-C20-H25    | 0.64      |
| C2-C3-C4-C5   | 1.23      | C17-N13-C28- C30 | -179.65   | C18-C20-C24-C22    | 0.22      |
| N12-C3-C4-C5  | 176.95    | H16-N14-C15-N13  | 160.69    | H25-C20-C24-C22    | 179.99    |
| C4-C3-N12-C15 | 121.24    | C15-N14-C30-C28  | -9.11     | C19-C22-C24-H27    | -179.72   |
| H9-C4-C5-C6   | 178.88    | H16-N14-C30-C28  | -159.56   | N13-C28-C30-N14    | 5.66      |
| C4-C5-C6-Br11 | -179.68   | N13-C17-C18-C20  | 179.53    | O29-C28-C30-N14    | -174.5    |

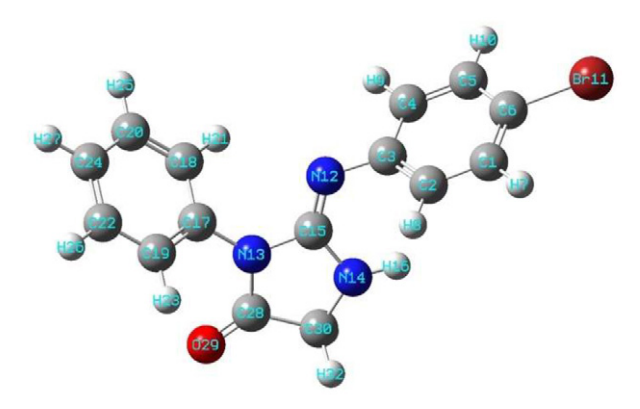


**Figure 5.** Optimized structure of the potent compound **13b** DFT-B3LYP/6-311++G(d,p).

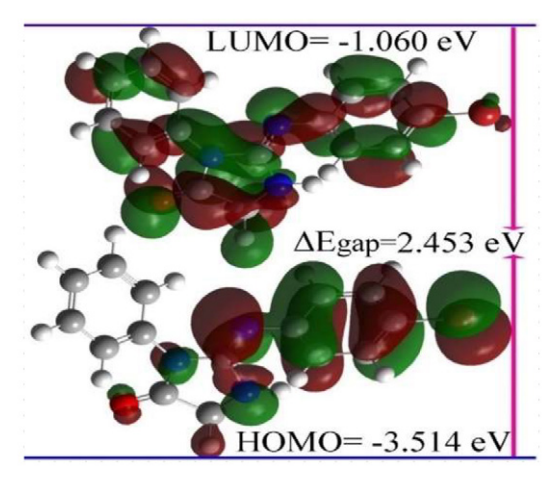


**Figure 6.** HOMO-LUMO surfaces with  $\Delta E_{ga}$  of the potent **13b** computed at DFT-B3LYP/6-311++G(d,p) combination.

### Table 6. Values of homo-lumo, $\delta e_{gap}$ and reactivity parameters of potent compound 13b computed at dft-b3lyp/6-311++g(d,p)

| Property           | Formula                               | Value  |
|--------------------|---------------------------------------|--------|
| LUMO energy        | E <sub>L</sub> (eV)                   | -1.060 |
| HOMO energy        | $E_{H}(eV)$                           | -3.514 |
| Energy gap         | $\Delta E_{gap} = E_{L} - E_{H} (eV)$ | 2.453  |
| hardness           | $\eta = (E_L - E_H)/2 \text{ (eV)}$   | 1.227  |
| Softness           | $\zeta = 1/\eta \text{ (eV}^{-1})$    | 0.815  |
| Chemical potential | $\mu = (E_L + E_H)/2 \text{ (eV)}$    | -2.287 |
| Electronegativity  | $\chi = -\mu \text{ (eV)}$            | 2.287  |
| Electrophilicity   | $\psi = \mu^2/2\eta \text{ (eV)}$     | 2.132  |

#### 4. Conclusions

To summarize, our work involved design and synthesis of two compound series featuring imidazolidine-2,4-dione as well as thiazolidine-2,4-dione structural elements. The synthesized compounds have demonstrated notable cytotoxicity against the tested cancer (Caco-2) cell lines. The two most potent compounds were compound 13b and compound 13c. The activity values of these compounds against the Caco-2 cell line were 41.30  $\pm$  0.07  $\mu M$  and 109.2  $\pm$  0.027  $\mu M$ , respectively. The compounds 13b and 13c, which exhibited the highest activity, had selective index values of 12.03 and 7.38, respectively. This indicates that the compounds had a good therapeutic window and significant anticancer selectivity. To validate its promise as a clinically effective anticancer treatment, more mechanis-

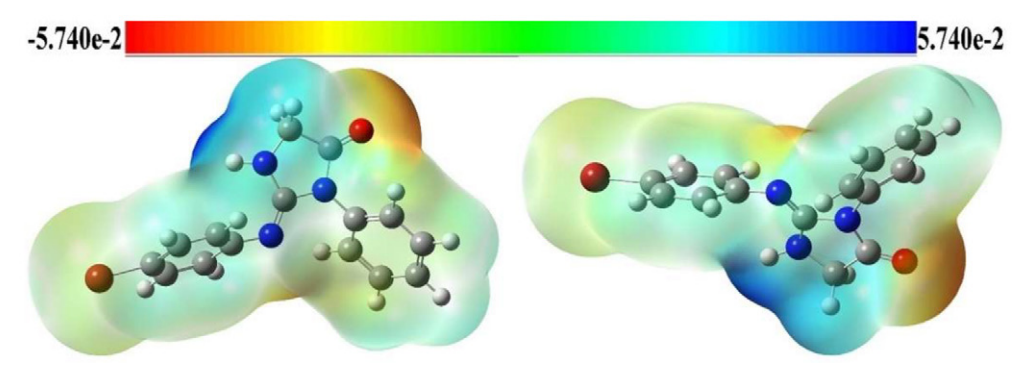


Figure 7. MEP of the potent molecule1 obtained by DFT-B3LYP/6-311++G(d.p) level

tic research, *in vivo* validation, and drug formulation improvement are required.

#### 5. References

- Z. Tarhini, J. Magne, P. Preux, A. Parenté, M. Mathonnet, N. Christou, J. Jost, *Biomed. Pharmacother.* 2024, *170*, 115950.
   DOI:10.1016/j.biopha.2023.115950
- D. Sonkin, A. Thomas, B. A. Teicher, Cancer Genet. 2024, 286–287, 1–11. DOI:10.1016/j.cancergen.2024.06.001
- K. Bukowski, M. Kciuk, R. Kontek, *Int. J. Mol. Sci.* 2020, 21(9), 3233. DOI:10.3390/ijms21093233
- 4. N. Kumar, N. Goel, Anti-Cancer Agents Med. Chem. 2022, 22(20), 3196–3207.
  - **DOI:**10.2174/1871520622666220404082648
- Y. Wan, G. Fang, H. Chen, X. Deng, Z. Tang, Eur. J. Med. Chem.
   2021, 226, 113837. DOI:10.1016/j.ejmech.2021.113837
- A. Jaromin, A. Czopek, S. Parapini, N. Basilico, E. Misiak, J. Gubernator, A. Zagórska, *Biomolecules* 2020, 11(1), 33. DOI:10.3390/biom11010033
- D. Bialonska, J. K. Zjawiony, Mar. Drugs 2009, 7(2), 166–183.
   DOI:10.3390/md7020166
- G. Bansal, S. Singh, V. Monga, P. V. Thanikachalam, P. Chawla, *Bioorg. Chem.* 2019, 92, 103271.
   DOI:10.1016/j.bioorg.2019.103271
- Y. Komatsu, T. Yoshino, K. Yamazaki, S. Yuki, N. Machida, T. Sasaki, I. Hyodo, Y. Yachi, H. Onuma, A. Ohtsu, *Invest. New Drugs* 2014, 32(3), 473–480.
   DOI:10.1007/s10637-013-0056-3
- M. Azizmohammadi, M. Khoobi, A. Ramazani, S. Emami, A. Zarrin, O. Firuzi, R. Miri, A. Shafiee, *Eur. J. Med. Chem.* 2013, 59, 15–22. DOI:10.1016/j.ejmech.2012.10.036
- S. Chandrappa, C. V. Kavitha, M. S. Shahabuddin, K. Vinaya, C. A. Kumar, S. R. Ranganatha, S. C. Raghavan, K. S. Rangappa, *Bioorg. Med. Chem.* 2009, *17*(6), 2576–2584.
   DOI:10.1016/j.bmc.2009.01.066
- F. Damkaci, A. A. Szymaniak, J. P. Biasini, R. Cotroneo, *Compounds* 2022, 2 (3), 182–190.
   DOI:10.3390/compounds2030015
- 13. H. Kumar, A. Deep, R. K. Marwaha, *BMC Chem.* **2020**, *14*, 25. **DOI**:10.1186/s13065-020-00678-2
- M. Al-Ghorbani, M. A. Gouda, M. Baashen, O. Alharbi, F. A. Almalki, L. V. Ranganatha, *Pharm. Chem. J.* 2022, 56(1), 29–37. DOI:10.1007/s11094-022-02597-z
- E. S. Tantawy, A. M. Amer, E. K. Mohamed, M. M. Abd Alla, M. S. Nafie, *J. Mol. Struct.* **2020**, *1210*, 128013.
   **DOI:**10.1016/j.molstruc.2020.128013
- G. M. Morris, R. Huey, W. Lindstrom, M. F. Sanner, R. K. Belew, D. S. Goodsell, A. J. Olson, *J. Comput. Chem.* 2009, 30(16), 2785–2791. DOI:10.1002/jcc.21256
- M. N. Khadri, H. A. Khamees, S. Kouser, S. A. Khanum, J. Mol. Struct. 2023, 1272, 134240.
  - **DOI:**10.1016/j.molstruc.2022.134240
- F. H. Al-Ostoot, H. A. Khamees, N. Prasad, F. Zameer, S. A. Khanum, J. Mol. Struct. 2022, 1270, 133963.

- **DOI:**10.1016/j.molstruc.2022.133963
- M. Jyothi, H. A. Khamees, S. M. Patil, R. Ramu, S. A. Khanum, *J. Iran. Chem. Soc.* 2022, *19*, 3919–3933.
   DOI:10.1007/s13738-022-02574-z
- 20. B. B. Touré, K. Miller-Moslin, N. Yusuff, L. Perez, M. Doré, C. Joud, W. Michael, L. DiPietro, S. Van Der Plas, M. McEwan, F. Lenoir, M. Hoe, R. Karki, C. Springer, J. Sullivan, K. Levine, C. Fiorilla, X. Xie, R. Kulathila, K. Herlihy, D. Porter, M. Visser, ACS Med. Chem. Lett. 2013, 4, 186–190.

DOI:10.1021/ml300321d

- Y. Gu, M. Chen, B. H. May, X. Liao, J. Liu, L. Tao, D. M. Sze,
   A. L. Zhang, S. Mo, *Phytomedicine* 2018, 51, 214–225.
   DOI:10.1016/j.phymed.2018.10.004
- G. M. Morris, D. S. Goodsell, R. S. Halliday, R. Huey, W. E. Hart, R. K. Belew, A. J. Olson, *J. Comput. Chem.* **1998**, *19*, 1639–1662.
  - **DOI:**10.1002/(SICI)1096-987X(19981115)19:14<1639::AID -JCC10>3.0.CO;2-B
- L. L. C. Schrodinger, The PyMOL Molecular Graphics System, Version 1.8, 2015.
- 24. D. S. Biovia, Discovery Studio Visualizer, 2017.
- P. Hohenberg, W. Kohn, *Phys. Rev.* **1964**, 136, B864–B871.
   **DOI:**10.1103/PhysRev.136.B864
- V. L. Ranganatha, C. Mallikarjunaswamy, R. Ramu, P. S. Shirahatti, N. Kumar, B. P. Sowmya, H. A. Khamees, M. Madegowda, S. A. Khanum, *Bioinformation* 2021, 17, 393.
- G. Naray-Szabo, M. R. Peterson, J. Mol. Struct.: Theochem 1981, 85, 249–255. DOI:10.1016/0166-1280(81)85023-3
- H. A. Khamees, M. Jyothi, S. A. Khanum, M. Madegowda, *J. Mol. Struct.* 2018, 1161, 199–217.
   DOI:10.1016/j.molstruc.2018.02.045
- 29. M. Frisch, Gaussian 09, Revision D.01, 2009.
- K. El-Adl, H. Sakr, S. S. A. El-Hddad, A. A. El-Helby, M. Nasser, H. S. Abulkhair, *Arch. Pharm.* 2021, 354, 2000491.
   DOI:10.1002/ardp.202000491
- M. R. Mohamed, W. R. Mahmoud, R. H. Refaey, R. F. George,
   H. H. Georgey, ACS Med. Chem. Lett. 2024, 15, 892–898.
   DOI:10.1021/acsmedchemlett.4c00095
- N. S. Hanafy, N. A. A. M. Aziz, S. S. A. El-Hddad, M. A. Abdelgawad, M. M. Ghoneim, A. F. Dawood, S. Mohamady, K. El-Adl, S. Ahmed, *Arch. Pharm.* 2023, 356, 2300137.
   DOI:10.1002/ardp.202300137
- 33. M. Al-Ghorbani, Russ. *J. Org. Chem.* **2022**, *58*, 1272–1279. **DOI:**10.1134/S1070428022090123
- O. Alharbi, K. A. Al-Mutairi, M. M. Ibrahim, R. Ramu, M. Al-Ghorbani, *Chem. Biodivers.* 2025, e202402104.
   DOI:10.1002/cbdv.202402104
- H. Boulebd, J. Biomol. Struct. Dyn. 2022, 40, 10373–10382.
   DOI:10.1080/07391102.2021.1943529
- 36. T. Mosmann, *J. Immunol. Methods* **1983**, *65*, 55–63. **DOI:**10.1016/0022-1759(83)90303-4
- M. Türkmenoğlu, S. T. Yıldırım, A. Altay, B. Türkmenoğlu, *ChemistrySelect* 2024, 9, e202303519.
   DOI:10.1002/slct.202303519
- A. Tomberg, Gaussian 09W Tutorial: An Introduction to Computational Chemistry Using G09W and Avogadro Soft-

- ware, 2013, 1-36.
- Ł. Balewski, M. Gdaniec, A. Hering, C. Furman, A. Ghinet,
   J. Kokoszka, A. Ordyszewska, A. Kornicka, *Int. J. Mol. Sci.* 2024, 25, 11495. DOI:10.3390/ijms252111495
- N. T. A. Ghani, A. M. Mansour, Eur. J. Med. Chem. 2012, 47, 399–411. DOI:10.1016/j.ejmech.2011.11.008
- T. Prashanth, V. Lakshmi Ranganatha, M. Al-Ghorbani, S. Girish, H. A. Khamees, S. A. Khanum, *Discov. Chem.* 2025, 2, 19. DOI:10.1007/s44371-025-00089-z
- Y. Wang, Y. Zhong, Y. Wang, Y. Ma, X. Gao, L. Xu, J. He, K. Yung, X. Li, L. Wu, W. Wong, CCS Chem. 2024, 1–13.
   DOI:10.31635/ccschem.024.202404867
- R. I. Al-Wabli, K. S. Resmi, Y. S. Mary, C. Y. Panicker, M. I. Attia, A. A. El-Emam, C. Van Alsenoy, *J. Mol. Struct.* 2016, 1123, 375–383. DOI:10.1016/j.molstruc.2016.07.044
- 44. Y. Erdogdu, D. Manimaran, M. T. Güllüoğlu, M. Amalanathan, I. Hubert Joe, S. Yurdakul, *Opt. Spectrosc.* **2013**, *114*, 525–536. **DOI**:10.1134/S0030400X13040073

#### **Povzetek**

Sintetizirali smo derivate tiazolidin-2,4-diona in imidazolidin-2,4-diona. Tiazolidin-2,4-dion 3 je bil pripravljen z uporabo kloroocetne kisline in tiouree, nato pa kondenziran s tereftalaldehidom za tvorbo 4-((2,4-dioksotiazolidin-5-ilidensko)metil)benzaldehida 4. Ta spojina je reagirala z 2-ariloksiacetohidrazidi 8a in 8b in dala Schiffove baze 9a-b. Imidazolidin-2,4-dioni 13a-c so bili sintetizirani s ciklizacijo anilinov 10a-c, sečnine 11 in kloroocetne kisline 12. Spojine 9a-b in 13a-c so bile ovrednotene glede protitumorske aktivnosti proti celični liniji Caco-2, pri *čemer* sta spojini 13b in 13c izkazali najmočnejšo jakost (vrednosti IC $_{50}$  41,30 ± 0,07  $\mu$ M in 109,2 ± 0,027  $\mu$ M). Izvedeni so bili DFT-izračuni, vključno z analizo HOMO-LUMO, oceno energijske vrzeli in molekularnim dokovanjem, z namenim ovrednotenja in optimizcije molekulskih lastnosti ciljnih spojin.



Except when otherwise noted, articles in this journal are published under the terms and conditions of the Creative Commons Attribution 4.0 International License